CrystEngComm

New cocrystals of ezetimibe with L-proline and Imidazole

Journal:	*CrystEngComm*
Manuscript ID:	CE-ART-06-2014-001127.R1
Article Type:	Paper
Date Submitted by the Author:	15-Jul-2014
Complete List of Authors:	Shimpi, Manishkumar; Luleå Technical University, Health Science Childs, Scott; 1Renovo Research, Boström, Dan; Umeå University, Thermal Energy Conversion Laboratory, Department of Applied Physics and Electronics Velaga, Sitaram; Luleå Univeristy of Technology,

Journal Name

RSCPublishing

ARTICLE

New cocrystals of ezetimibe with L-proline and imidazole

Cite this: DOI: 10.1039/x0xx00000x

Manishkumar R. Shimpi,[a+] Scott L. Childs,*[b+] Dan Boström[c] and Sitaram P. Velaga*[a]

Received 00th January 2012,
Accepted 00th January 2012

DOI: 10.1039/x0xx00000x

www.rsc.org/

The objectives of the study were to screen and prepare cocrystals of anti-cholesterol drug ezetimibe (**EZT**) with the aim of increasing its solubility and dissolution rate. Thermodynamic phase diagram based high throughput screening was performed using wet milling/grinding or solution crystallization methods. A large number of coformers were tested and the resulting solids were preliminarily characterized using X-ray powder diffraction (PXRD) and Raman spectroscopy. Potential cocrystals of **EZT** with L-proline and imidazole and a solvate formamide were identified in the screening experiments. The cocrystal hits were further characterized by differential scanning calorimetry (DSC), thermogravimetric analysis (TGA), solution Proton nuclear magnetic resonance spectroscopy (^{1}H-NMR) and single crystal XRD. The dissolution properties and stability of cocrystals were determined. Single-crystal X-ray diffraction data were obtained for **EZT**, **EZT-IMI** cocrystal and formamide solvate of ezetimibe. All three systems were crystallized in non-centrosymmetric orthorhombic space group $P2_12_12_1$ with Z =4. Robust O–H···O, O–H···N, N–H···O and C–H···O hydrogen bonds played an important role in all these crystal structures. **EZT-PRO** cocrystal showed improved apparent solubility and solid state stability.

Journal Name RSCPublishing

ARTICLE

Introduction

Active pharmaceutical ingredients (APIs) in the form of crystalline materials are the preferred solid forms in oral dosage forms. Physical properties of crystalline materials depend on the packing of molecules in the crystal lattice and interactions among them. Currently, pharmaceutical scientists employ different strategies to alter the crystal structure to obtain desired properties of APIs.[1, 2] A detailed understanding of interactions in a given molecule is prerequisite for designing new crystalline form. In this context, crystal engineering has emerged as an important tool in the design of new solids.[3] A substantive definition of crystal engineering is provided by Desiraju in 1989 as "Crystal engineering mainly deals with the understanding of intermolecular interactions and utilization of such understanding in the design of new solids with desired physical and chemical properties".[4] Crystal engineering encompasses the idea of establishing strong and directional interactions in new compounds based on the synthon approach to altering the molecular arrangement in the crystal.

Design of molecular assemblies based on hydrogen bonding and other interactions has emerged as a powerful tool in the discovery of pharmaceutical cocrystals.[5-7] Pharmaceutical cocrystals, often relying on the formation of hydrogen bonds between an API and one or more additional molecular components (coformers), are a relatively new class of pharmaceutical materials.[8-11] Cocrystals have emerged as a promising means to modify physical (solubility, dissolution, thermal stability, etc.) and mechanical properties of API's.[12] By cocrystallizing an API or a salt of an API with a coformer (neutral molecule), one can create a new solid state form with unique properties relative to the existing solid forms of the API or its salt. In pharmaceutical research, cocrystal approach has been mainly employed to increase the solubility, dissolution rate and bioavailability of poorly water soluble drug molecules while maintaining a stable crystalline form. For example, cocrystals of danazol,[13] indomethacin,[14] itraconazole,[15] piroxicam,[16] fluoxetine HCl,[17] caffeine,[18] norfloxacin[19] and carbamazepine,[20] with diverse coformers have been designed with improved solubility/dissolution and bioavailability.

Ezetimibe, 1-(4-fluorophenyl)-3-[3-(4-fluorophenyl)-3-hydroxypropyl]-4-(4-hydroxyphenyl)-2-azetidinone, (Figure 1) is a hypocholesterolemic agent used in the treatment and/or prevention of atherosclerosis reduction of plasma cholesterol levels. Ezetimibe (**EZT**) is the first class of new compounds that selectively inhibits the intestinal absorption of cholesterol and related phytosterols causing reduced blood cholesterol levels.[21-23]

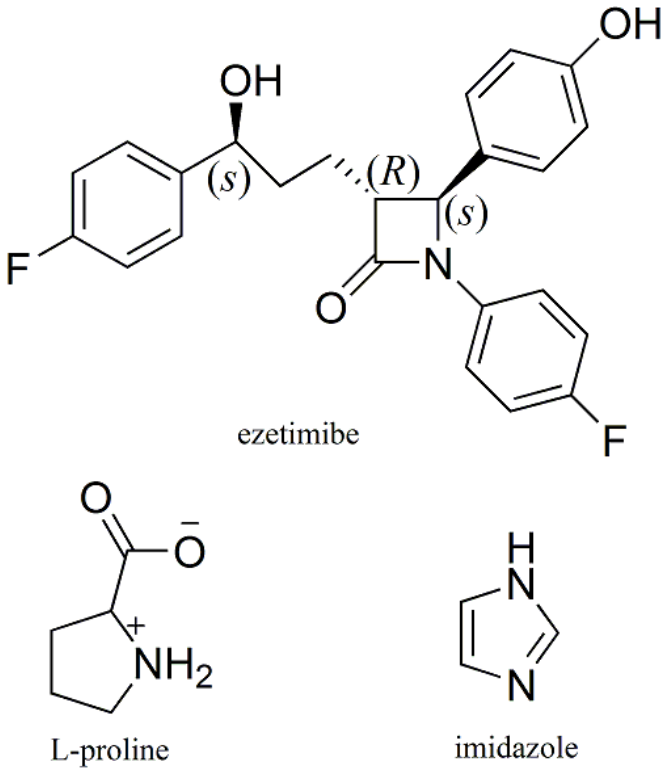

Fig. 1 Molecular structure of chiral ezetimibe [1-(4-fluorophenyl)-3-[3-(4-fluorophenyl)-3-hydroxypropyl]-4-(4-hydroxyphenyl)-2-azetidinone] and coformers.

EZT is a highly lipophilic molecule having log *P* (octanol/water) of 4.5. Due to its high hydrophobic character, it exhibits very low bioavailability (35-65%). **EZT** is weakly acidic in nature containing ionizable groups ($pK_a \sim 9.48$) and virtually insoluble in aqueous media but shows good intestinal permeability (i.e. BCS class II drug). This property is a common obstacle in the drug development that can be solved by converting active drug molecules into pharmaceutically acceptable salts or solid dispersion or cocrystals with desirable physico-chemical properties. A broad array of formulation strategies can be found in the literature for improving oral bioavailability of **EZT**. Examples of these approaches include solid dispersions[24-27] liquid solid technique,[28] nanosuspensions,[29] emulsions,[30] and particle sizing approaches such as nanocrystals.[31]

The objectives of this work were to screen for new cocrystals of **EZT** using advanced rational techniques, characterize and evaluate their properties, including dissolution behavior and stability.

Experimental

All chemicals and solvents (Purity > 99%) were purchased from Sigma Aldrich or Acros Organics and were used without further purification.

High-Throughput (HT) cocrystal screening

The approximate solubility of **EZT** was determined in twelve solvents by adding aliquots of solvent to a weighed amount of the API. The solubility data was used to select solvents or solvent mixtures for cocrystal experiments that would create systems in which both the API and coformer were saturated. Care was taken to make sure that excess solids of both components were present in the screening experiments. A large set of coformers were selected based on toxicity, structure complementary, and pKa. High throughput screening experiments were conducted in two stages. In stage one, saturated solution (reaction crystallization) experiments using non-stoichiometric amounts of API and coformer were conducted. In stage two, stoichiometric amounts of API and coformer were wet milled. XRPD data was collected on all solids isolated from screening experiments.

Preparation of ezetimibe-L-proline cocrystal (EZT-PRO)

A 7 mL glass vial was charged with 101.7 mg (0.24 mmol) of ezetimibe, 28 mg (0.24 mmol) of L-proline. 3 mL of a ethyl acetate:heptane: 2,2,2-trifluoro ethanol (1:3:0.5, vol:vol) solvent mixture was added to form a slurry. This reaction was stirred and after 12 hours 3 mL of heptane was added. The reaction was allowed to stir for a total of 72 hours, at which time the solids present were isolated by vacuum filtration and air dried at room temperature to yield 110 mg (84%) of ezetimibe-L-proline cocrystal.

Preparation of ezetimibe-imidazole cocrystal (EZT-IMI)

A PEEK grinding jar was charged with 81.0 mg (0.19 mmol) of ezetimibe and 13.3 mg (0.19 mmol) of imidazole. 150 µL of 1:3 (v:v) ethyl acetate: heptane were added along with two stainless steel grinding balls. The grinding jar was shaken at 80% power on a Retsch MM2 grinding apparatus for two 10 minute periods. The solvent was then evaporated and the dry powder was isolated to yield 75 mg (80%) of the ezetimibe:imidazole (**EZT-IMI**) cocrystals.

Growing single crystals of different forms

Crystallization of ezetimibe anhydrate (**EZT**): Single crystal was formed by slow evaporation of saturated solution of **EZT** in 2,2,2-trifluoroethanol.
Ezetimibe-imidazole cocrystal (**EZT-IMI**): Cocrystal powder (50 mg) was dissolved in 4 mL of acetonitrile in a 10 mL conical flask. Single crystals were prepared from slow evaporation of acetonitrile at room temperature in a fume hood.
Crystallization of ezetimibe-formamide (**EZT-FOR**): Large single crystals were obtained from a slow evaporation of a saturated solution of ezetimibe in formamide.

Ball-mill grinding

Solid-state grinding in manual experiments was performed with a Retsch MM200 Mixer Mill equipped with 10 mL stainless steel grinding jars and two 7 mm stainless steel grinding balls per jar. All grinding was performed at a rate of 30 Hz. The external temperature of the grinding jars at the conclusion of the grinding experiments did not exceed ca. 30 °C.

Raman spectroscopy

The Raman spectra were recorded on a Chromex Sentinel dispersive Raman unit equipped with a 785nm, 70 mW excitation laser and a TE cooled CCD. Each spectrum is a result of twenty co-added 20 second scans. The unit has continuous automatic calibration using an internal standard. The data was collected by SentinelSoft data acquisition software and processed in GRAMS AI.

Infrared spectroscopy

Infrared spectra were recorded on a Bruker Vertex 80v FTIR spectrometer equipped with a DLaTGS detector and a Platinum-ATR accessory with a diamond crystal as ATR element. Both a single beam background without sample and single beam spectra of the powered samples were obtained by averaging 128 scans with an optical resolution of 4 cm^{-1}. The resulting interferograms were Fourier transformed using the Mertz phase correction mode, a Blackman-Harris 3-term apodization function, and a zero filling factor of 2. All spectra were recorded under vacuum using the double-side forward-backward acquisition mode.

Differential scanning calorimetry (DSC)

Thermal analyses of cocrystal samples were performed on a TA instruments DSC Q1000. The sample was placed into an aluminum DSC pan, and the weight accurately recorded. The pan was crimped and the contents heated under nitrogen atmosphere. Indium was used as the calibration standard. The data was collected in duplicate for each sample. At cocrystal screening stage, thermal analysis was performed on a TA instruments differential scanning calorimeter 2920.

Thermogravimetric (TG) analysis

TG analyses were performed using a TA Instruments 2950 thermogravimetric analyzer. Each sample was placed in an aluminum sample pan and inserted into the TG furnace. Nickel and Alumel^{TM} were used as the calibration standards. Reported temperatures are at the transition maxima.

Powder X-ray diffraction (PXRD)

PXRD patterns were collected on a Scintag X1 powder diffractometer equipped with a peltier cooled solid state detector. Data were collected using Cu-Kα radiation (1.54056 Å). The tube voltage and amperage were set at 45 kV and 40 mA, respectively. Samples were prepared for analysis by pressing a thin layer of the sample onto a metal sample holder. Instrument calibration was performed using a quartz reference standard.

Single-crystal X-ray diffraction

The single-crystal X-ray diffraction data of the crystals were collected on a Bruker Nonius Kappa CCD. The data set for compounds were collected at room temperature (293 K). The crystals were quite stable and hence no extraordinary precautions were necessitated for the smooth collection of intensity data. All the data sets were collected using Mo $K\alpha$ radiation (λ= 0.71073 Å), and crystal structures were solved by direct methods using SIR-92 and refined by full-matrix least-squares refinement on $F2$ with anisotropic displacement parameters for non-H atoms using SHELXL-2013. Hydrogen

atoms were placed on their expected chemical positions using the HFIX command. All the non-hydrogen atoms were refined anisotropically. Structure solution, refinement, and generation of publication materials were performed by using shelXLe, V623 software.[32] Table 1 gives the pertinent crystallographic data, and the hydrogen-bond parameters respectively. All the intermolecular interactions were computed using PLATON.[33] All packing diagrams are generated using Diamond software.[34]

Table 1 Crystallographic data and structure refinement parameters of **EZT, EZT-IMI, EZT-FOR**.

	EZT	**EZT-IMI**	**EZT-FOR**
empirical formula	$C_{24}H_{21}F_2N_1O_3$	$C_{27}H_{25}F_2N_3O_3$	$C_{25}H_{24}F_2N_2O_4$
formula wt	409.42	477.50	454.46
crystal shape	plates	plates	plates
crystal color	colorless	colorless	colorless
crystal system	orthorhombic	orthorhombic	orthorhombic
space group	$P2_12_12_1$	$P2_12_12_1$	$P2_12_12_1$
a(Å)	5.9510(2)	5.8320(2)	6.1400(2)
b(Å)	15.899(5)	15.7520(5)	17.0770(7)
c(Å)	21.400(2)	25.6730(1)	21.3500(1)
V(Å^3)	2024.8(2)	2358.47	2238.61(2)
Z	4	4	4
D_{calc} (g cm^{-3})	1.343	1.345	1.348
T (K)	293(2)	293(2)	293(2)
λ($Mo_{K\alpha}$)[Å]	0.71073	0.71073	0.71073
μ (mm^{-1})	0.101	0.099	0.103
F(000)	856	1000	952
No. unique reflns	2755	3237	2749
No. reflns used	1585	2150	1791
No. parameters	273	326	324
GOF on F^2	1.061	1.046	1.148
$R1[I>2\sigma(I)]$	0.0561	0.06	0.0551
$wR2$	0.1549	0.1994	0.1341
CCDC No.	947148	947149	947150

Dissolution experiment

The dissolution media was prepared by dissolving 1.74 g of NaOH, 19.77 g of $NaH_2PO_4.H_2O$ or 17.19 g of anhydrous NaH_2PO_4, and 30.93 g of NaCl in 5 L of purified water. The pH was adjusted to approximately 6.5 by adding a solution of NaOH or HCl as necessary. Tween-80 was added to form a 1.3% by weight Tween-80 solution. Sodium dodecyl sulfate (SDS) was added to form a 0.2% by weight SDS solution. The samples used in the dissolution experiments were passed through a 75 micron sieve prior to charging the dissolution vessel with the solid. 1.5 g of the sieved formulated sample was charged to an empty 1 liter USP dissolution flask. 500 mL of dissolution media were added and the stirring rate was set at 70 RPM. The temperature of the dissolution bath was maintained between 20 and 21 degrees Celsius. Approximately 1 mL samples were withdrawn at 0.5, 1, 1.5, 2, 3, 5, 10, 15, 30, 60, and 120 minutes. Samples were immediately filtered and diluted with an equal volume of methanol. The concentration of **EZT** was determined by HPLC.

Results and discussion

HT screening and cocrystal preparation

More systematic and efficient high-throughput crystallization systems had been developed in the recent years to screen and identify new cocrystal solid forms.[35] In this work, high-throughput screening experiments were conducted using two complementary crystallization techniques, reaction crystallization and wet milling (a.k.a solvent drop grinding). High-throughput cocrystal screening using reaction crystallization and solvent drop grinding had been demonstrated for several previously reported cocrystals.[36] In the reaction crystallization technique, empirical solubility data for cocrystal components in a given solvent or solvent mixture is used to design experimental conditions that will allow for the transformation of single components into cocrystals if a cocrystal exists and is nucleated.

Our approach to cocrystal screening was to create experimental conditions under which the cocrystal will be the thermodynamically stable solid form. Thus, if the cocrystal exists and nucleates, then the cocrystal will be recovered in the solids isolated. In order to avoid relying on kinetic conditions to create cocrystals in screening experiments, we had used sealed (non-evaporating) reactions with a fixed solvent, API and coformer composition. If both the API and coformer are saturated with excess solid present, then the cocrystal will be formed if nucleation is not a limiting factor. In successful experiments, the solid formed was often a mixture of cocrystal and either the API or coformer. Careful selection of the solvent composition and volume such that the solubility of API and coformer are similar will optimize the ternary phase diagram of the system and produce a larger percentage of cocrystal in the screening experiments.[37] In HT wet milling experiments the stoichiometry of the components was fixed at 1:1, 2:1 or 1:2 and the volume and composition of the solvent was varied to produce the desired reaction conditions. In reaction crystallization a stirred slurry or suspension of the API and coformer is created in a solvent or solvent mixture and the saturation of the components is assured by the addition of excess API and coformer. The overall composition of the reaction crystallization experiment is non-stoichiometric, but if the stoichiometric ratio of the excess solids is correct, pure cocrystal can be formed.[38]

Solid-state characterization

Primary analyses of solid-state samples had been performed by PXRD and Raman spectroscopy. Both PXRD and Raman spectroscopy are versatile, non-destructive, noninvasive and complementary analytical methods to characterize materials. PXRD patterns for **EZT**, L-proline, **EZT-PRO**, imidazole and **EZT-IMI** are shown in Figure 2. The diffraction patterns of the cocrystals were found to be distinctly different as compared to the starting material, indicating the formation of new solids that are different from the **EZT** and coformers.

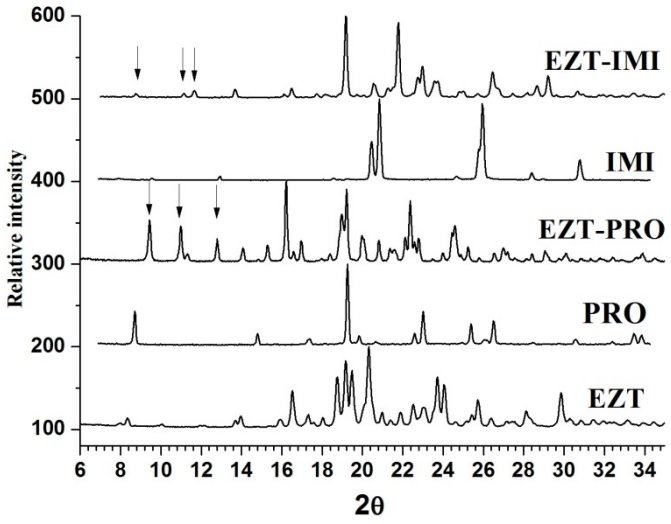

Fig. 2 Powder X-ray diffraction patterns for cocrystal of **EZT-PRO** and **EZT-IMI**.

The Raman spectra of new solid forms obtained in the screening were compared with that of **EZT** and coformers. Generally, the vibrational spectra of polymorphs, cocrystals, salts and solvates are distinct, and spectral analysis can be used to differentiate solid forms.[39, 40] These comparisons can provide evidence to cocrystal formation due to changes in the intermolecular interactions. The Raman spectra in the region of 800 to1800 cm^{-1} for **EZT**, L-proline and **EZT-PRO** cocrystal are presented in the Figure 3. In cocrystals, the C=O and C–N bands of **EZT** were shifted to lower or higher wavenumber, which suggests that the molecular environment around these groups has changed in the solid state. The Raman spectra for pure **EZT** showed strong bands at 1610, 1400 and at 1216 cm^{-1} corresponding to C=O stretching, C–N stretching and O–H in plane bending, respectively. In the cocrystal spectra, these bands had shifted to 1611, 1390 and 1223 cm^{-1}, respectively. The shifting of C=O (stretching), and C–N (stretching), wavenumber of **EZT** indicates that the carbonyl group is participating in hydrogen bonding.

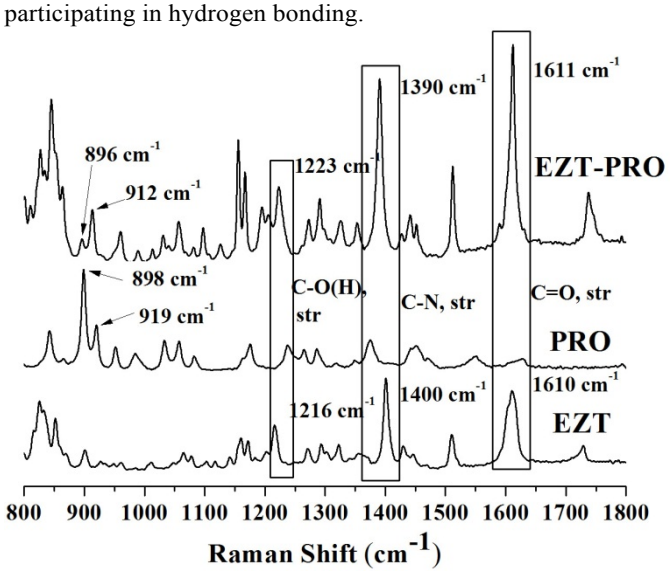

Fig. 3 Raman spectra for (a) **EZT**, (b) L-proline, and (c) **EZT-PRO** cocrystal.

Raman spectrum of L-proline is in agreement with the literature.[41, 42] The spectrum of pure L-proline showed strong band at 898 and 919 cm^{-1} corresponding to ring stretching and variation of COO^- group that appears as a broad band at 896 cm^{-1} and 912 cm^{-1} in cocrystal. This is probably due to the involvement of COO^- group in the intermolecular hydrogen bonding with OH group of **EZT**. Moreover, the L-proline molecule is typically present in the form of a zwitterion forming N^+–H O^- bonds in the crystal structure.[43] The spectroscopic and crystal structure analyses suggested that L-proline most probably exists as a zwitterion in the crystal lattice of **EZT-PRO** with the carboxylate group of L-proline interacting with OH group of **EZT**.

The Raman spectra for **EZT**, imidazole and **EZT-IMI** cocrystal are presented in Figure 4. A comparison of the spectra had revealed that there are several band shifts occurring between individual components and the cocrystal. The strong band in pure **EZT** at 1610 cm^{-1} was a broad peak with decreased intensity in the cocrystal. The strong peaks at 1400 and 1216 cm^{-1} corresponding to pure **EZT** were shifted to 1394 cm^{-1} and 1204 cm^{-1} respectively with decrease in the intensity in the **EZT-IMI** cocrystal. The strong band at 1263, and 1448 cm^{-1} corresponding to C–N (stretching) and N–H (stretching), respectively, were present in pure imidazole. In cocrystals, these bands have appeared at 1260 and 1444 cm^{-1} respectively with decrease in the intensity. Moreover, band at 1323 cm^{-1} in pure imidazole spectrum has disappeared in the cocrystal spectra. These observations indicate that the N–atoms of imidazole form hydrogen bonds with **EZT** resulting in the cocrystal.

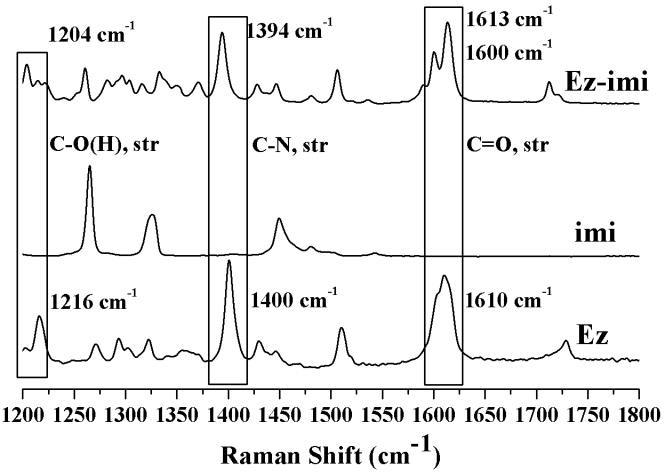

Fig. 4 Raman spectra for (a) **EZT**, (b) imidazole, and (c) the **EZT-IMI** cocrystal.

Infrared spectroscopy is powerful tool to understand the hydrogen bonding in organic multicomponent systems.[44] Strong IR absorptions in the region 1550-1620 cm^{-1} are typical of the asymmetric stretching mode of the COO^- group and weaker absorptions around 1400 cm^{-1} arise from the symmetric COO^- stretching mode. Figure 5 shows IR spectra of **EZT**, L-proline and **EZT-PRO**. The spectrum of L-proline shows strong band at 1613 cm^{-1} corresponds to the asymmetric COO^- stretching mode[42] which shifted to 1605 cm^{-1} in solid state spectrum of **EZT-PRO**. The most interesting finding was the disappearance of the symmetric COO^- band of L-proline at 1406 cm^{-1} which probably indicated the breaking O-H…O=C bond of **EZT** upon formation of its cocrystals. In **EZT** spectrum, bands at 3434 and 3254 cm^{-1} assigned to OH stretching. Whereas, in the cocrystal, these bands had appeared at 3471 and 3128 cm^{-1}

which indicates that O-H group is involved in the intermolecular hydrogen bonds with L-proline molecules.

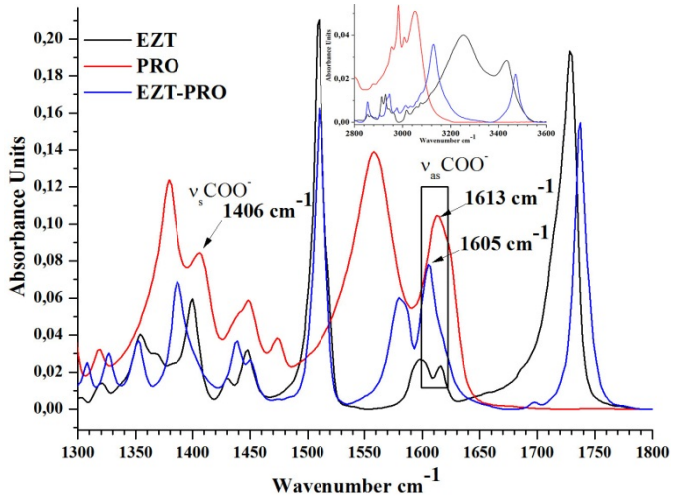

Fig. 5 Comparison between IR spectra of **EZT-PRO** cocrystal and its components with COO- stretching region, and the O-H stretching region (inset).

The characteristic strong C=O stretching band at 1714 cm^{-1} of **EZT-IMI** indicates presence of intermolecular interactions. This was confirmed with SXRD (Figure 12b) where carbonyl group forms C–H···O (H···O = 2.03 Å, C···O = 2.95 Å, C–H···O = 173°) hydrogen bond with imidazole. Several characteristic new vibrational features have been recorded in the IR spectra of **EZT-IMI** (Figure 6).

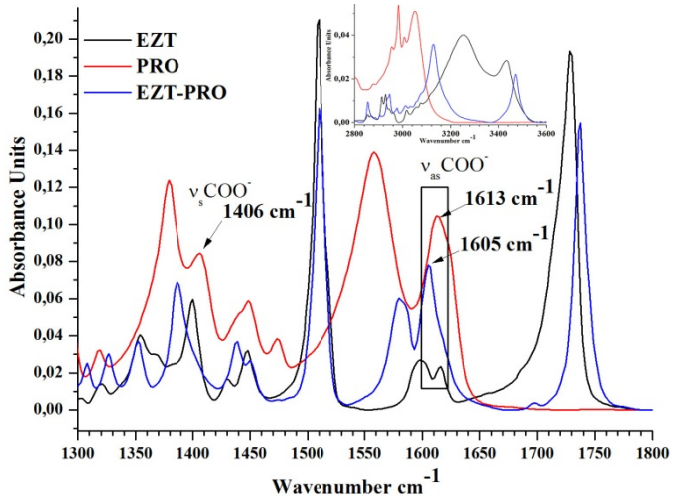

Fig. 6 The IR spectra of **EZT**, **IMI** and **EZT-IMI**, in the wavenumber range (1300-1800 and 2200-3600 cm^{-1}).

Thermal analysis has been widely used in the characterization of polymorphs, salts and cocrystals, where changes in thermal properties of solids are examined with respect to temperature.[19] DSC and TGA thermograms for the starting materials and cocrystals have been presented in the Figure 7. Starting materials, **EZT**, L-proline and imidazole showed onset of melting at ~ 165 °C, 229 °C and 91 °C, respectively. The melting behavior of **EZT** is in agreement with the literature.[31] Whilst cocrystals, **EZT-PRO** and **EZT-IMI** showed a single endothermic transition, attributed to melting phenomenon at T_{onset} ($T_{max;}$ ΔH_f) at 174.22°C ±1.6 (175.98 °C ± 1.3; 101.34 J/g ±13) and T_{onset} ($T_{max;}$ ΔH_f) at 124.83°C ±0.81 (126.53 °C ± 0.4; 115.1 J/g ±8) respectively and no other transitions were observed. It can also be noted that the cocrystals melt in the temperature range between API and coformers. In fact, the melting behavior of these cocrystals is similar to that of number of cocrystals reported in the literature.[45] TGA of these new phases shows mass loss after melting points, which is attributable to degradation of the cocrystals (Figure S4). It also indicates that both cocrystals are thermally stable until the melting point.

Solution ^{1}H-NMR was used to identify and confirm the ratio of **EZT** and the coformers in the cocrystal systems. ^{1}H-NMR indicates both the components are present in 1:1 molar ratio and are chemically intact.

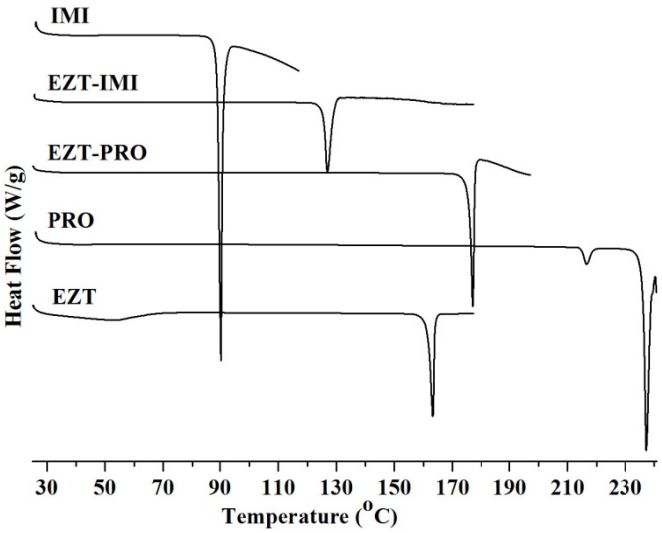

Fig. 7 DSC thermograms of **EZT**, **PRO**, **IMI**, **EZT-PRO** and **EZT-IMI**.

Crystal structure analyses

The crystal structure of **EZT** anhydrate[46] and monohydrate[47] are known in the literature, which were determined from powder diffraction structure analysis and single-crystal structure analysis, respectively. In this study, **EZT** was recrystallized in different solvents and solvent mixtures to obtain single crystals for XRD analysis. Good quality crystals of **EZT** anhydrate and **EZT**-formamide (**EZT-FOR**) solvates were obtained from 2,2,2-trifluoroethanol and formamide respectively. Cocrystals of **EZT-IMI** were obtained by slow evaporation from acetonitrile at room temperature. However, we were not successful in growing single crystals of **EZT-PRO** despite intense efforts following rational approaches. Hence, this section deals with the crystal structure analysis of **EZT** anhydrate, **EZT-IMI** and **EZT-FOR** solvate which provide insights on the crystal packing and intermolecular interactions. The crystals of these solid forms are as shown in the Figure 8.

Fig. 8 Optical micrographs of the crystals **EZT** (a), **EZT-IMI** (b), **EZT-FOR** (c).

(a) Ezetimibe anhydrate (EZT)

The **EZT** anhydrate crystallized in the orthorhombic $P2_12_12_1$ space group with one molecule in the asymmetric unit (Figure S1). The crystal structure reported here is quite similar to the structure solved from the powder diffraction data.[46] The 4-fluorophenyl moiety linked to N-atom is almost coplanar to the azetidinone ring (torsion angle C11–N1–C19–C20 = 179.5°). The angle between the plane of 4-fluorophenyl moiety and 4-hydroxyphenyl moiety is 78.68(2)°. The crystal structure of **EZT** contains O–H···O mediated synthons formed by hydroxyl groups (aromatic and aliphatic) interact with carbonyl groups. The 4-fluorophenyl moiety participates in intramolecular C–H O (H···O = 2.57 Å, C O = 3.1390 Å, C-H O = 120°) hydrogen bonding with the carbonyl oxygen atom of azetidinone ring (torsion angle (C12–N1–C19–C24 = 161.04°). The crystal structure analysis shows that aliphatic hydroxyl group is involved in two distinct intermolecular hydrogen bonds (Figure 9a), one between aromatic hydroxyl group and aliphatic hydroxyl group O–H-O (H-O = 2.01 Å, O-O = 2.7752 Å, O–H-O = 155°) and second one between aliphatic hydroxyl group and carbonyl group of azetidinone (O–H-O (H-O = 2.04 Å, O-O = 2.7425 Å, O–H O = 143°). Packing arrangement of **EZT** is shown in Figure 9b. Overlapped **EZT** molecules are held by weak hydrogen bonds.

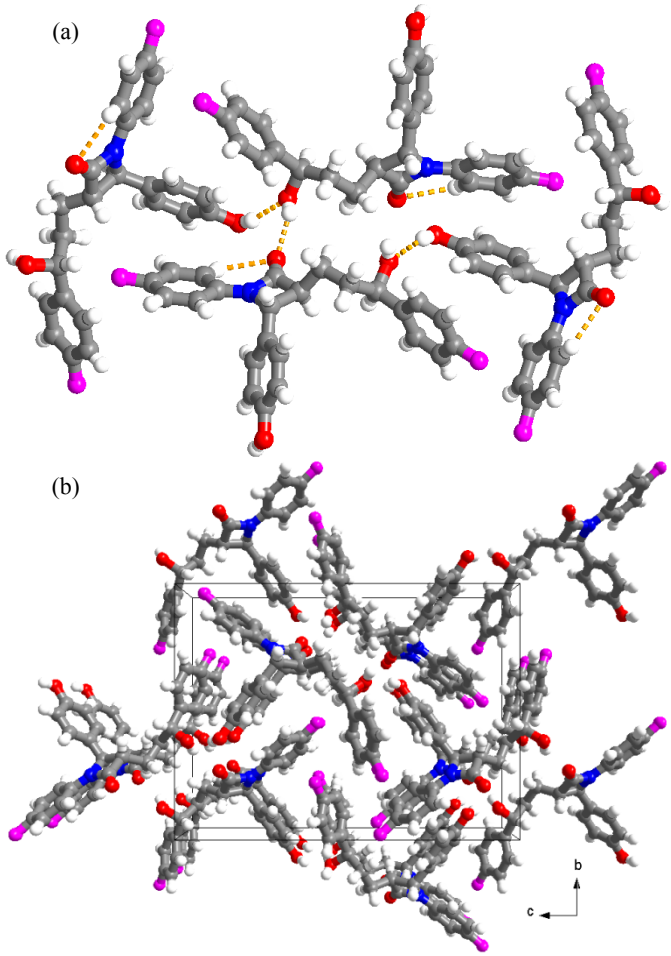

Fig. 9 (a) intermolecular O–H···O and intramolecular C–H···O hydrogen bonds in **EZT** anhydrate. (b) packing diagram showing the arrangement of **EZT** along *a*-axis.

(b) Ezetimibe-imidazole (EZT-IMI)

The 1:1 ezetimibe-imidazole cocrystal (**EZT-IMI**) crystallized in orthorhombic $P2_12_12_1$ space group, with one molecule of each of **EZT** and imidazole in the asymmetric unit (Figure S2). The orientation of 4-fluorophenyl and 4-hydroxyphenyl moieties with the azetidinone ring is slightly changed (torsion angle C12–N3–C19–C20 = -163.6° and angle between the plane is 75.21°) in the cocrystal as compared to **EZT** anhydrate. The major difference between **EZT** and **EZT-IMI** is the conformation of the 3-(4-fluorophenyl)-3-hydroxypropyl fragment. The torsion angle C10–C9–C8–C7 of -178.90(3)° in **EZT-IMI** is considerably smaller than the corresponding angle in the anhydrate (82.73(5)°).

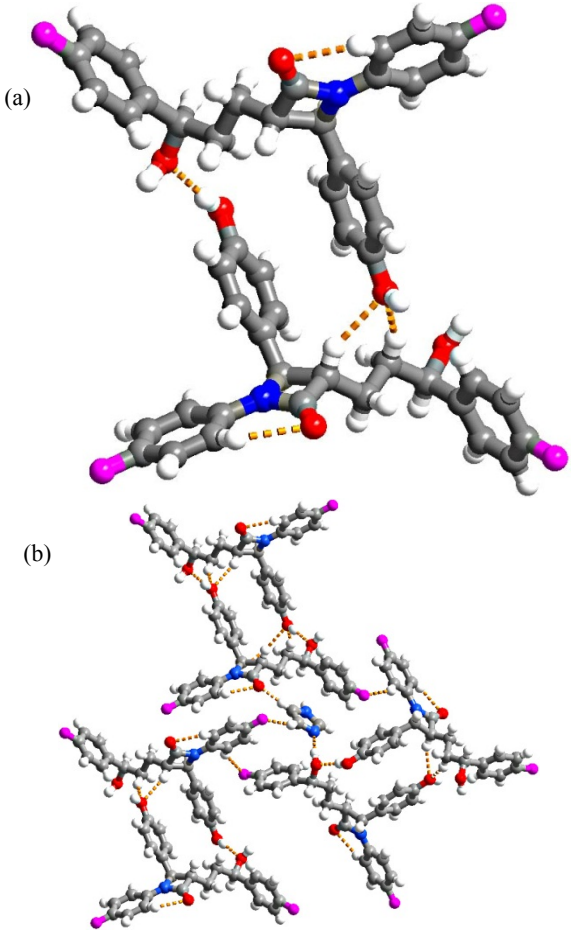

Fig. 10 (a) Molecular recognition pattern between **EZT** molecule in **EZT-IMI** cocrystal (b) interactions of guest imidazole molecule with host **EZT** molecules.

Further, **EZT** molecules form dimers by O–H-O (H-O = 1.85Å, O-O = 2.6383 Å, O–H O = 160°), C–H O (H O = 2.45Å, C-O = 3.3448 Å, C–H-O = 155°) and C–H-O (H-O = 2.56Å, C-O = 3.4213 Å, C–H-O = 150°) hydrogen bonds as shown in Figure 10a. These dimeric interactions of **EZT** molecules exist due to different orientation of 3-(4-fluorophenyl)-3-hydroxypropyl fragment, to accommodate the additional imidazole molecule. Three dimeric units of **EZT** molecules are assembled in such a way that it forms the channels, which are occupied by imidazole molecules as shown in Figure 10b. These dimeric units are involved in weak C–H-F interactions leading to the formation of host-guest frameworks (Figure 11). In the crystal structure, N-atom of imidazole acts as a hydrogen bond

acceptor and C–H acts as a hydrogen bond donor. Interestingly, N–H group of imidazole does not participate in hydrogen bonding. The aliphatic hydroxyl group forms strong hydrogen bonding with imidazole via O–H-N (H-N= 1.81Å, O-N = 2.7219 Å, O–H-N = 169°).

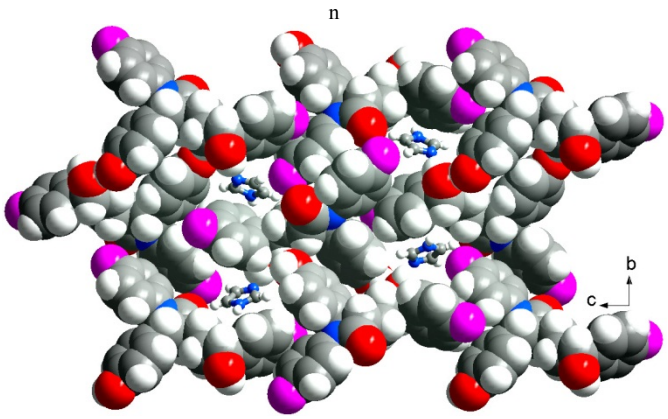

Fig. 11 Host-guest framework viewed along a-axis. The guest imidazole molecules are shown in ball and stick for clarity.

(c) Ezetimibe-formamide (EZT-FOR)

The **EZT-FOR** is crystallized in the orthorhombic $P2_12_12_1$ space group with one molecule each of **EZT** and formamide in the asymmetric unit (Figure S3). The crystal structure analysis reveals that the orientation of the 3-(4-fluorophenyl)-3-hydroxypropyl fragment in **EZT** is similar to the orientation in **EZT** anhydrate. The aliphatic hydroxyl group and 4-hydroxyphenyl group are above and below the plane of **EZT** molecules. The three dimensional packing arrangement of **EZT-FOR** is similar to that of anhydrous **EZT** (Figure 12a). Interestingly, **EZT** molecules adopt the stacked layered structure along the *a*-axis held together by aliphatic hydroxyl group and carbonyl group of azetidinone ring via O–H-O (H-O = 1.94 Å, O-O = 2.7552 Å, O–H-O = 174°) hydrogen bonds as shown in Figure 12b. Interestingly, in **EZT-FOR**, the hydrogen bond between aliphatic hydroxyl and carbonyl remains, but the formamide replaces hydrogen bonding between aromatic hydroxyl and aliphatic hydroxyl groups. The closer examination of the crystal structure shows that formamide molecules are involved in hydrogen bonding with aliphatic hydroxyl, aromatic hydroxyl and carbonyl oxygen atoms of **EZT** molecules via N–H-O (H-O = 2.11 Å, N-O = 2.9366 Å, N–H-O = 162^O); O–H-O (H-O = 1.88 Å, O-O = 2.6989 Å, O–H-O = 176°) and C–H-O (H-O = 2.59 Å, C-O = 3.4579 Å, C–H-O = 156°) interactions (Figure 12c).

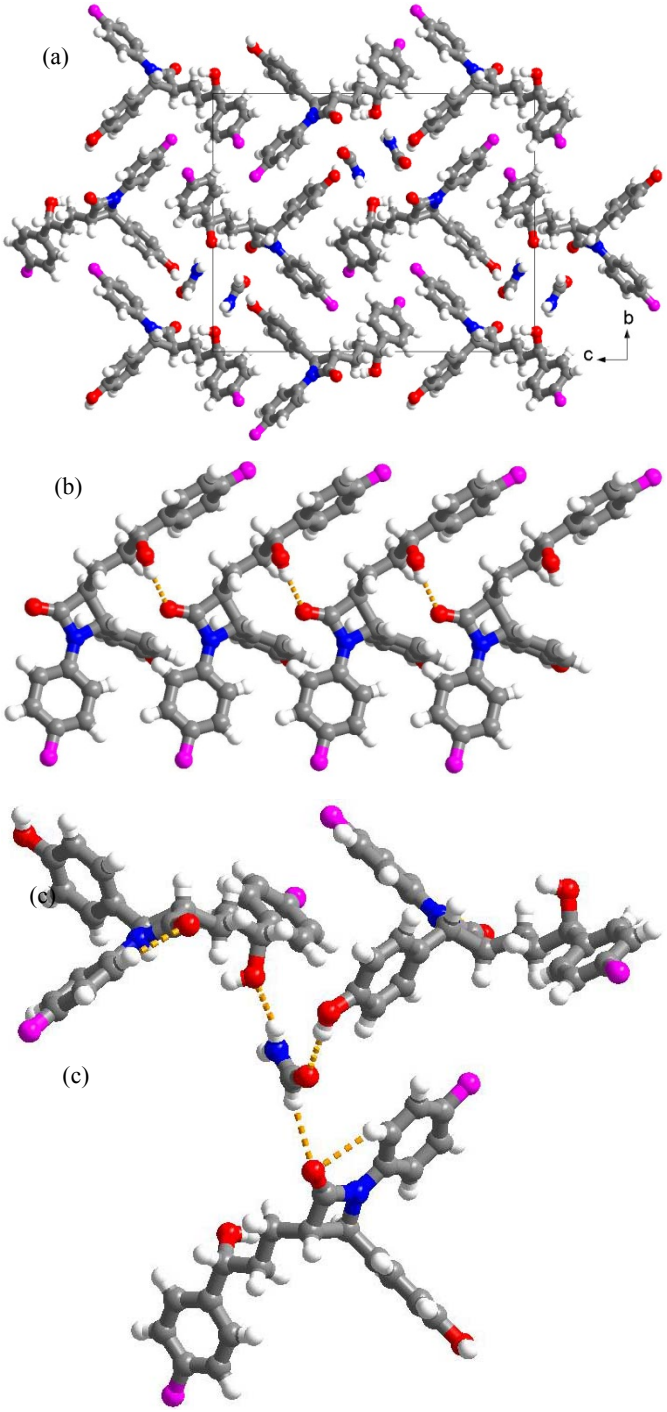

Fig. 12 (a) The packing diagram view along *a*-axis (b) stacking of **EZT** molecules with O–H-O interactions. (c) Interactions of formamide with three **EZT** molecules in crystal structure of **EZT-FOR**. Note the intramolecular C–H-O hydrogen bond in the **EZT** molecule.

Powder dissolution and stability study

The inclusion of a more water soluble coformer in the cocrystal of a poorly soluble API will typically result in the cocrystal with a higher solubility and dissolution rate compared to the single component crystal of the API.[48] The resulting cocrystal will generate solution levels of the API that are supersaturated relative to the poorly soluble crystalline form of the API. A powder dissolution experiment can reveal information about a cocrystal's ability to generate and maintain supersaturated conditions. The ability to create and maintain supersaturation

levels using a danazol cocrystal is linked to improved bioavailability in rats.[13]

Powder dissolution experiments were carried out on **EZT-PRO** cocrystal at 20°C. These results are presented in the graphical form in Figure 13. The data for the cocrystal was normalized such that the solution concentration of **EZT** (mM) is plotted for both systems. Within the first minute, the concentration of **EZT** from the cocrystal was five times higher than from the **EZT** formulation. The peak concentration of **EZT** from the cocrystal was 0.29 mg/mL in 3 minutes compared to 0.13 mg/mL after 30 minutes for the API. After 2 hours the concentration of **EZT** in the cocrystal experiment was still 1.5 times higher than the **EZT** experiment. The enhanced solubility of **EZT-PRO** cocrystal is similar to the spring and parachute type behavior.[49] Further, the **EZT-PRO** cocrystal was stored in an RH environment of approximately 75% relative humidity (saturated NaCl) at 40 °C for 31 days. The PXRD data indicates no substantial change in the solid form of the sample occurred during the course of experiment (Figure S6).

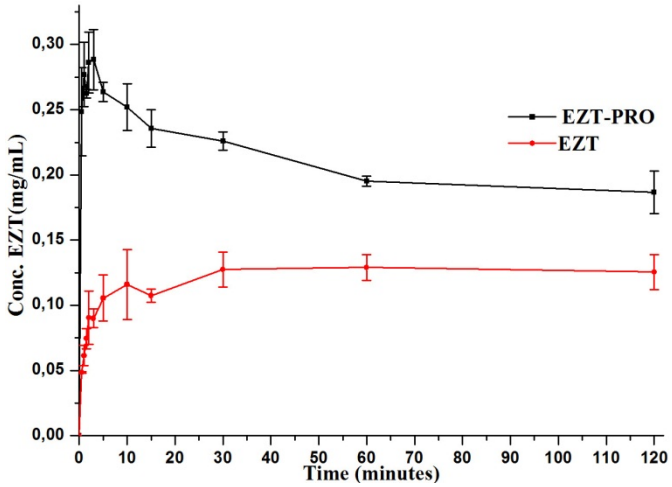

Fig. 13 Powder dissolution profiles for **EZT** and **EZT-PRO** cocrystal in phosphate buffer pH6.5 at 20 °C.

Conclusions

Two new cocrystals of ezetimibe have been discovered and thoroughly characterized using relevant solid-state characterization tools. The single crystal structures of ezetimibe and its cocrystal and solvate with imidazole and formamide respectively have been solved. The structural analysis has revealed O–H-O, O–H-N, N–H-O and C–H-O interactions played an important role in the assemblies of ezetimibe and its cocrystal and solvate. Further, the ezetimibe-L-proline cocrystal, has showed rapid dissolution and higher supersaturation compared to ezetimibe anhydrate. In fact, these cocrystals were stable at accelerated stability conditions. Thus, the design of pharmaceutical cocrystals can offer many opportunities in the drug development and delivery.

Acknowledgements

M.S and S.V is grateful to the Kempe foundation for postdoctoral grant.

Notes

[a]Department of Health Sciences Luleå University of Technology, S-971 87, Luleå, Sweden.
[b]Renovo Research, Atlanta, GA 30316, USA.
[c]Thermal Energy Conversion Laboratory, Department of Applied Physics and Electronics, Umeå University, Umeå S-90187, Sweden.
+Equal contribution
Corresponding authors: Scott L. Childs and Sitaram P. Velaga

† Footnotes should appear here. These might include comments relevant to but not central to the matter under discussion, limited experimental and spectral data, and crystallographic data.

Electronic Supplementary Information (ESI) available: **Fig. S1** ORTEP of asymmetric unit in the crystal lattice of Ezetimibe, **EZT**; **Fig. S2** Asymmetric unit of **EZT-IMI** cocrystal; **Fig. S3** ORTEP diagram of the **EZT-FOR**.; Thermal ellipsoids are drawn at the 50 % probability level. **Fig. S4** TGA plot for (a) **EZT-PRO** and (b) **EZT-IMI** cocrystals; **Fig. S5** ^{1}H-NMR plot for (a) **EZT-PRO** and (b) **EZT-IMI** cocrystals; **Fig. S6** XRPD of **EZT-PRO** before RH experiment (bottom) and after 31 days at 40 ºC 75%RH (top). **Table S1** Characteristics (distances/Å and angles/º) of hydrogen bonds in the molecular compounds and crystallographic cif files. CCDC 947148-947150. See DOI: 10.1039/b000000x/

References

1 N. Schultheiss and A. Newman, *Cryst. Growth Des.,* 2009, **9**, 2950-2967.
2 B. Rodriguez-Spong, C. P. Price, A. Jayasankar, A. J. Matzger and N. Rodriguez-Hornedo, *Adv. Drug Delivery Rev.,* 2004, **56**, 241-274.
3 G. R. Desiraju, *Angew. Chem. Int. Ed.,* 1995, **34**, 2311-2327.
4 G. R. Desiraju, *Crystal Engineering. The Design of Organic Solids*, Elsevier, Amsterdam, 1989.
5 S. Basavoju, D. Bostroem and S. P. Velaga, *Pharm. Res.,* 2008, **25**, 530-541.
6 A. Alhalaweh, L. Roy, N. Rodriguez-Hornedo and S. P. Velaga, *Mol. Pharmaceutics,* 2012, **9**, 2605-2612.
7 S. Karki, T. Friscic, W. Jones and W. D. S. Motherwell, *Mol. Pharmaceutics,* 2007, **4**, 347-354.
8 H. G. Brittain, *J. Pharm. Sci.,* 2013, **102**, 311-317.
9 S. L. Childs and M. J. Zaworotko, *Cryst. Growth Des.,* 2009, **9**, 4208-4211.
10 N. Shan and M. J. Zaworotko, *Drug Discovery Today,* 2008, **13**, 440-446.
11 A. Nangia, *J. Chem. Sci.,* 2010, **122**, 295-310.
12 Ö Almarsson and M. J. Zaworotko, *Chem. Commun.,* 2004, 1889-1896.
13 S. L. Childs, P. Kandi and S. R. Lingireddy, *Mol. Pharmaceutces,* 2013, **10**, 3112-3127.
14 M. Jung, J. Kim, M. Kim, A. Alhalaweh, W. Cho, S. Hwang and S. P. Velaga, *J. Pharm. Pharmacol.,* 2010, **62**, 1560-1568.
15 J. F. Remenar, S. L. Morissette, M. L. Peterson, B. Moulton, J. M. MacPhee, H. R. Guzman and O. Almarsson, *J. Am. Chem. Soc,* 2003, **125**, 8456-8457.
16 S. L. Childs, G. P. Stahly and A. Park, *Mol. Pharmaceutics,* 2007, **4**, 323-338.
17 S. L. Childs, L. Chyall, J. Dunlap, V. Smolenskaya, B. Stahly and G. Stahly, *J. Am. Chem. Soc.,* 2004, **126**, 13335-13342.
18 A. Trask, J. van de Streek, W. Motherwell and W. Jones, *Cryst. Growth Des.,* 2005, **5**, 2233-2241.
19 S. Basavoju, D. Boström and S. P. Velaga, *Cryst. Growth Des.,* 2006, **6**, 2699-2708.
20 M. B. Hickey, M. L. Peterson, L. A. Scoppettuolo, S. L. Morrisette, A. Vetter, H. Guzmán, J. F. Remenar, Z. Zhang, M. D. Tawa, S. Haley,

M. J. Zaworotko and O. Almarsson, *Eur. J. Pharma. Biopharma.,* 2007, **67**, 112-119.
21 A. Husain, M. M. Alam, M. S. Azim, M. Mitra and P. S. Bhasin, *J. Pharm. Res.,* 2012, **5**, 4056-4059.
22 M. J. M. Darkes, R. M. Poole and K. L. Goa, *Am. J. Cardiovasc. Drugs,* 2003, **3**, 67-76.
23 M. van Heek and H. Davis, *Eur. Heart J. Suppl.,* 2002, **4**, J5-J8.
24 K. R. Parmar, S. R. Shah and N. R. Sheth, *Dissolution Technol.,* 2011, **18**, 55-61.
25 P. P. Sancheti, P. Karekar, V. M. Vyas, M. Shah and Y. V. Pore, *Pharmazie,* 2009, **64**, 227-231.
26 A. N. Sagri, R. A. Rub, A. S. Kulkarni, I. Gonjari, D. S. Saindane and U. I. Shaikh, *Asian J. Res. Chem.,* 2009, **2**, 325-331.
27 T. Taupitz, J. B. Dressman and S. Klein, *Eur. J. Pharm. Biopharm.,* 2013, **84**, 208-218.
28 R. Gudikandula, M. Kalla, S. R. Thakkalapally, A. Veeramalla and R. P. Indarapu, *Int. J. Pharm. Sci. Res.,* 2013, **4**, 3229-3238.
29 S. Mishra, D. S. Panda, M. Pradhan and I. Hussain, *J. Adv. Pharm. Res.,* 2011, **2**, 185-189.
30 J. T. Lalwani, V. T. Thakkar and H. V. Patel, *Int. J. Pharm. Pharm. Sci.,* 2013, **5**, 513-522.
31 T. Gulsun, R. N. Gursoy and L. Oner, *Chem. Pharm. Bull.,* 2011, **59**, 41-45.
32 32 C. B. Hubschle, G. M. Sheldrick and B. Dittrich, *J. Appl. Crystallogr.,* 2011, **44**, 1281-1284.
33 A. L. Spek, *J. Appl. Crystallogr.,* 2003, **36**, 7-13
34 Crystal-mpact, Brandenburg & Putz, Bonn, 2008.
35 S. L. Morissette, O. Almarsson, M. L. Peterson, J. F. Remenar, M. J. Read, A. V. Lemmo, S. Ellis, M. J. Cima and C. R. Gardner, *Adv. Drug Delivery Rev.,* 2004, **56**, 275-300.
36 J. Aaltonen, M. Alleso, S. Mirza, V. Koradia, K. C. Gordon and J. Rantanen, *Eur. J. Pharm. Biopharm.,* 2009, **71**, 23-37.
37 A. Alhalaweh, S. George, S. Basavoju, S. L. Childs, S. A. A. Rizvi and S. P. Velaga, *CrystEngComm,* 2012, **14**, 5078-5088.
38 N. Rodriguez-Hornedo, S. J. Nehm, K. F. Seefeldt, Y. Pagan-Torres and C. J. Falkiewicz, *Mol. Pharmaceutics,* 2006, **3**, 362-367.
39 H. R. H. Ali, A. Alhalaweh and S. P. Velaga, *Drug Dev. Ind. Pharm.,* 2013, **39**, 625-634.
40 H. G. Brittain, *Cryst. Growth Des.,* 2009, **9**, 3497-3503.
41 J. J. Cárcamo, A. E. Aliaga, E. Clavijo, C. Garrido, J. S. Gómez-Jeria and M. M. Campos-Vallette, *J. Raman Spectrosc.,* 2012, **43**, 750-755.
42 Z. Nengwu, P. Long, L. Haiming and W. R. Robinson, *Spectroscopy Letters,* 1997, **30**, 61-70.
43 R. L. Kayushina and B. K. Vainshtein, *Kristallografiya,* 1965, **10**, 834-844.
44 A. Mukherjee, S. Tothadi, S. Chakraborty, S. Ganguly and G. R. Desiraju, *CrystEngComm,* 2013, **15**, 4640-4654.
45 D. J. Good and N. Rodriguez-Hornedo, *Cryst. Growth Des.,* 2009, **9**, 2252-2264.
46 J. Bruening, E. Alig and M. U. Schmidt, *Acta Crystallogr., Sect. C: Cryst. Struct. Commun.,* 2010, **66**, o341-o344.
47 K. Ravikumar and B. Sridhar, *Acta Crystallogr., Sect. E: Struct. Rep. Online,* 2005, **61**, o2907-o2909.
48 A. Alhalaweh, L. Roy, N. Rodríguez-Hornedo and S. P. Velaga, *Mol. Pharmaceutics,* 2012, **9**, 2605-2612.
49 N. J. Babu, A. Nangia, *Cryst. Growth Des.,* 2011, **11**, 2662-2679.

